INTERNATIONAL
Agrophysics
www.international-agrophysics.org

Int. Agrophys., 2023, 37, 51-58
doi: 10.31545/intagr/156086

DEM modelling of wood sawdust compaction and the breakage strength of pellets as determined by a diametral compression test**

Józef Horabik[1]*, *Maciej Bańda*[1], *Vlasta Vozárová*[2], *Ľubomír Kubík*[2], *and Mateusz Stasiak*[1]

[1]Institute of Agrophysics, Polish Academy of Sciences, Doświadczalna 4, 20-290 Lublin, Poland
[2] Faculty of Engineering, Slovak University of Agriculture, Trieda A. Hlinku 2, 949 76 Nitra, Slovak Republic

Received June 10, 2022; accepted October 26, 2022

A b s t r a c t. Sawdust from six wood species typical of Eastern Europe: beech (*Fagus* L.), birch (*Betula* L.), oak (*Quercus* L.), pine (*Pinus sylvestris* L.), poplar (*Populus* L.) and willow (*Salix* L.) with a moisture content of 8% were compacted at a compressive pressure of 120 MPa in a laboratory mould with a diameter of 10 mm. Diametral compression tests were performed to determine the mechanical strength of the pellets. Discrete element method simulations were performed to reproduce the compaction process and the mechanical reaction of the pellets to diametral compression. It was found that the difference between the bulk density of the compacted and the relaxed pellets decreased with increases in the breakage strength of a pellet. The DEM simulations reproduced well the experimental data of the diametral compression test.

K e y w o r d s: sawdust pellets, diametral compression, tensile strength, DEM

INTRODUCTION

Waste biomaterials have recently become important renewable energy resources (Kalinyan and Morey, 2010). These materials have a low bulk density. Therefore, densification is commonly applied to reduce the costs of storage and transport (Molenda *et al*., 2021). Biomaterials are densified into briquettes, pellets, or cubes depending on the type of material and intended use. Pelletization is the most popular method of increasing the density. Pellets are a suitable feedstock for the heat and power industries. Wood residues constitute valuable feedstocks for the production of energy, fuels, and chemicals (Hehar *et al*., 2014). Wood sawdust is a convenient substrate for pelleting (Whittaker and Shield, 2017). Sawdust has a low bulk density in the range of 100-200 kg m^{-3}. Pelletization increases the bulk density by up to 1 000-1 200 kg m^{-3}. This value is far above the bulk density of the intact wood block (400-700 kg m^{-3}) and close to that of the intact wood solid-phase density including closed pores (1 050-1 400 kg m^{-3}) (Shaw *et al*., 2009; Kretschmann, 2010; Horabik *et al*. (2021).

The strength and durability of the pellets depends on the forces that connect the particles together. The binding forces between the particles depend on their chemical, physical, and mechanical properties. The compaction pressure, temperature, particle size, and moisture content are all factors with the most substantial influence on particle binding. The compaction pressure increases the contact area between the particles, increased temperature activates their inherent binders or added binders and also increases the extent of plastic deformation of the thermoplastic particles. Particle size and its distribution are the most important parameters influencing pellet strength. The recommended particle size for obtaining a good quality of pellet is a fraction of

*Corresponding authors e-mail: j.horabik@ipan.lublin.pl
**This work was supported by the Operational Programme–Integrated Infrastructure, Project Drive4SIFood, No. 313011V336 – Demand-Oriented Research for the Sustainable and Innovative Food, co-financed by the European Regional Development Fund (2019-2023).

a millimetre. Its strength and durability are affected by constituents such as starch, protein, fibre, and fat (Kalinyan and Morey, 2009). The moisture content must be optimized for individual feed material, as it may increase or decrease the durability of the pellet. A higher moisture content can reduce friction by lubricating the biomass. Lower friction increases the effective compressive pressure and finally increases the durability of the pellets. The higher moisture content increases the extent of the relaxation of the pellets after formation, which decreases their durability. The optimum moisture content must be determined for a particular feedstock prepared for pelletization, for example, for pine it is between 6-13% (Whittaker and Shield, 2017).

The diametral compression test is a convenient method for determining the tensile strength of cylindrical samples of different materials. In recent times, this method has been applied widely in order to determine the mechanical strength of biomass pellets (Stasiak *et al*., 2017; Shaw *et al*., 2009; Larsson and Samuelsson, 2017; Song *et al*., 2020).

The discrete element method (DEM) which was introduced by Cundall and Strack (1979) was extended with the parallel bonded particle model (BPM) of Potyondy and Cundall (2004) which appears to be very useful in providing a particle scale insight into the bonding mechanisms. DEM simulations reproduced the results of the experimental tests of the pressure compaction of biomass very well (Ilic *et al*., 2018), in terms of the mechanical behaviour of pinewood chips in cyclic loading (Xia *et al*., 2019), durability (Mahajan *et al*., 2017), and the breakage strength of wood (Horabik *et al*., 2021) and biomass pellets (Gilvari *et al*., 2020). DEM modelling of the mechanical behaviour of compacted biomass requires further study in order to verify its applicability to different types of biomass and experimental conditions.

The aim of the present study was to explore the possibility of the numerical modelling of the compaction process of wood sawdust and the reconstruction of the stress-deformation relationship of pellets during diametral compression using DEM simulations.

MATERIALS AND METHODS

Sawdust from six wood species that are typical of Eastern Europe: beech (*Fagus* L.), birch (*Betula* L.), oak (*Quercus* L.), pine (*Pinus sylvestris* L.), poplar (*Populus* L.) and willow (*Salix* L.) were used for pelletization. The mean particle size that was determined with the use of a set of sieves was in the range from 0.355 for birch to 0.593 for poplar (Table 1). The moisture content (MC) of all sawdust samples was 8±0.7%.

The sawdust was pelletized in a high pressure compaction process with the use of a piston-and-mould with a diameter of 10 mm and a height of 25 mm. 0.5 g samples of sawdust without any additives were compacted up to a pressure of 120 MPa using a universal testing machine (Instron 7782, High Wycombe, UK). The downward speed of the piston was 0.033 mm s^{-1} (Molenda *et al*., 2021).

Table 1. Mean particle size of sawdust used for pelletization

Material	Mean particle size d_p (mm)
Beech	0.526±0.048a
Birch	0.355±0.028b
Oak	0.409±0.024b
Pine	0.375±0.026b
Poplar	0.593±0.080a
Willow	0.531±0.042a

Mean values in a column followed by the same letter are not significantly different at the 5% level.

Helium pycnometer (Ultrapyc 1200e, Quantachrome Instruments, Boynton Beach, FL, USA) was used to measure the solid-phase density of the intact wooden blocks of 40 mm in diameter and 70 mm in height, the ρ_w value and the ρ_s of the sawdust particles.

The bulk density of the intact wood (ρ_{bw}), the initial bulk density of the sawdust (just before densification) (ρ_{bs}), and of the pellets (ρ_{bp}), were determined using the mass and volume of the specimens. An electronic calliper with an accuracy of 0.01 mm was used to measure the diameter and height of the pellets just before the diametral compression. The initial height of the bulk of the sawdust in the mould was used to determine the initial bulk density of the sawdust. The current height of the bulk of the sawdust was used to determine the bulk density during the compaction process (ρ_b).

The diametral compression test was performed using a universal testing machine (Lloyd LRX, Advanced Test Equipment Corp., San Diego, CA, USA). The tests were performed in five replicates. The load cell with a range of 200 N and an accuracy of ±0.2 N was used to measure the compression load. The tensile strength, σ_f, was determined from formula (1):

$$\sigma_f = \frac{P_f}{\pi R_p t} = \sigma_{1,max} \ , \tag{1}$$

where: P_f is the failure load, R_p is the radius of the pellet, and t is its thickness (Fig. 1). The tensile strength, σ_f, was identified with the maximum tension principal stress in the direction perpendicular to the load direction in the centre of the cylindrical object, $\sigma_{1,max}$.

A statistical analysis of the results was performed using Statistica v. 10.0 software (StatSoft Inc., Kraków, Poland). The results were presented as mean values±the standard deviation. The statistical significance of the differences between the mean values was determined on the basis of a one-way analysis of variance with a significance level of 5%.

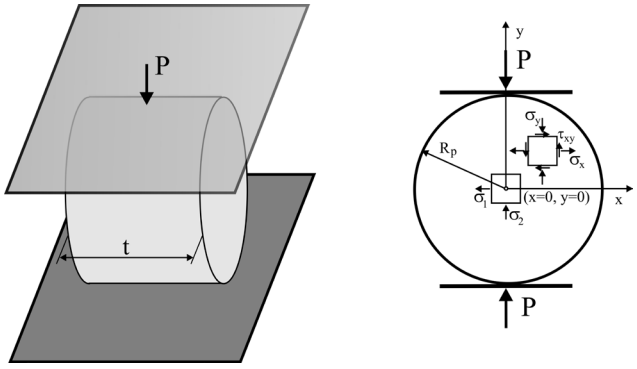

Fig. 1. The diametral compression test of the pellet with the indicated stress components.

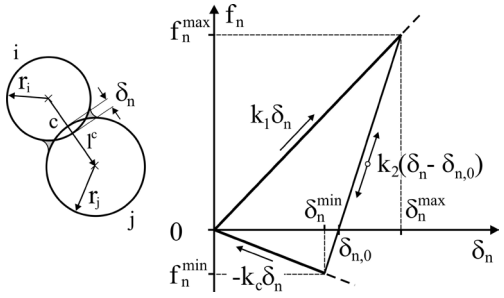

Fig. 2. Linear elastic-plastic contact model with the Bonded Particle Model.

The linear elastic-plastic contact model of Walton and Brown (1986) was applied to the simulations. For the compaction process, as well as the processes of unloading and removal from the mould, the model was extended with a linear adhesion as introduced by Luding (2005):

$$f_n = \begin{cases} k_1\delta_n & \text{loading} & k_2(\delta_n - \delta_{n,0}) \geq k_1\delta_n \\ k_2(\delta_n - \delta_{n,0}) & \text{unloading / reloading} & k_1\delta_n > k_2(\delta_n - \delta_{n,0}) > -k_c\delta_n \\ -k_c\delta_n & \text{unloading} & -k_c\delta_n \geq k_2(\delta_n - \delta_{n,0}) \end{cases}, \quad (2)$$

where: f_n is the contact normal force, k_1 is the loading stiffness, k_2 is the unloading stiffness, k_c is the adhesive stiffness, δ_n is the overlap in the normal direction, and $\delta_{n,0}$ is the residual overlap during unloading.

The plastic stiffness (k_1) was determined from the yield strength (p_y) of a particle using the following formula (DEM Solutions, 2018):

$$k_1 = 5r^* \min(p_{y,i}, p_{y,j}), \quad (3)$$

where: $r^* = r_i r_j/(r_i+r_j)$ is the equivaleradius of the particles in contact, and $p_{y,i}$ and $p_{y,j}$ are the yield strengths of particles i and j, respectively. The unloading stiffness k_2 was related to the loading stiffness k_1 by means of the restitution coefficient e (DEM Solutions, 2018):

$$e = \sqrt{\frac{k_1}{k_2}}. \quad (4)$$

The velocity-dependent dissipation of energy in the tangent direction followed the Tsuji *et al*. (1992) model related to the restitution coefficient e.

After relaxation, when the total kinetic energy was very low ($<10^{-8}$ J) and the overlap was close to the residual overlap ($\delta \sim \delta_{n,0}$), the adhesive interactions were replaced by the BPM model in order to bring the simulations closer to the experimental conditions of the breakage of bonds and to protect the particles from secondary adhesive bonds. To reduce the number of independent parameters of a bond it was assumed that the stiffness of the bond in the normal and tangent directions are the same and that the bond strength in the normal and tangent directions are also the same. Figure 2 presents the linear elastic-plastic contact model with a parallel bonded particle model. At $\delta_n = \delta_{n,0}$ the bond force equals zero. Any change in δ_n results in an increase in the tension force ($\delta_n - \delta_{n,0} < 0$) or in the compression force ($\delta_n - \delta_{n,0} > 0$) up to a limiting force (f_c), which leads to the breakage of the bond. Details concerning the applied mathematical formulas of BPM were presented in an earlier publication about DEM modelling of the breakage strength of wood sawdust pellets (Horabik *et al*., 2021).

Simulations were performed for the assembly of 40 000 spherical particles. The mean radius was 0.2 mm. The radii were normally distributed in the range of 0.14-0.26 mm. The solid density of the particles was assumed to be the density of the wood block (Xia *et al*., 2019). The coefficients of particle-particle and particle-wall friction were adopted from similar studies concerning biomass pellets (Gilvari *et al*., 2020) and pinewood chips (Xia *et al*., 2019). The Poisson ratio $v = 0.35$ and the coefficient of restitution $e = 0.5$ were in accordance with the typical values for wood materials (Kretschmann, 2010; Rackl *et al*., 2017). A yield strength of $p_y = 100$ MPa and a bond radius of $r_b = 20$ μm followed the findings of a study concerning the optimization of bond parameters for the compaction of wood sawdust samples performed by Horabik *et al*. (2021). The material parameters of the mould and sawdust particles, and the interaction parameters used in DEM simulations are shown collectively in Table 2. The values of the bond modulus of elasticity (E^b) and the bond strength (σ_c) were tested in order to provide the best fit of the $\sigma_1(\Delta L/D)$ relationship during diametral compression.

DEM simulations were performed in sequence and in the following stages: particle generation and filling, compaction, unloading, mould removing, relaxation, BPM initiation, and diametral compression (Horabik *et al*., 2021).

In order to reduce the computing time, the particle density was increased by a factor of 10^4 and accordingly, the acceleration due to gravity was reduced by a factor of 10^4 to maintain the force of gravity. The timestep of integration was of 2×10^{-6} s, *i.e*., 4% of the Rayleigh timestep (Huang *et al*., 2014). EDEM software was used for the simulations (DEM Solutions, 2018).

The relative root mean-square error (*RRMSE*) was used to evaluate the fitting quality of the experimental stress-deformation relationship $\sigma_1(\Delta L/D)$ through the DEM simulation:

$$RRMSE = \sqrt{\frac{1}{n}\sum_{i=1}^{n}\left(\frac{\sigma^i_{1,exp} - \sigma^i_{1,DEM}}{\sigma^i_{1,exp}}\right)^2}, \quad (5)$$

where: $\sigma^i_{1,\mathrm{exp}}$ is the experimental value of the tension stress, $\sigma^i_{1,DEM}$ is the DEM simulated tension stress, and n is the number of sampling of the $\sigma_1(\Delta L/D)$ relationship.

RESULTS

The mean particle size values of the sawdust d_p were in the range from 0.355 mm for birch to 0.593 mm for poplar (Table 1). The density of the solid phase of the intact wood ρ_w was in the range from 682.3 kg m^{-3} for poplar to 1 426.6 kg m^{-3} for pine (Table 3). The solid phase density of the sawdust particles ρ_s was in a much narrower range as compared to the intact wood. The lowest value was for birch (1 465 kg m^{-3}) and the highest one was for poplar (1 511 kg m^{-3}). The solid phase density of the sawdust particles was considerably higher than the solid phase density of the intact wood samples due to the destruction of the majority of closed pores inside the sawdust particles which are present inside the tissue of the intact wood samples. During the helium pycnometry test, it was found that the gas could easily penetrate the open pores inside the sawdust particles but it took longer to penetrate the closed pores inside the intact wood.

Table 2. DEM simulations parameters

Parametr	Symbol	Value
Container		
Radius (mm)	R	5
Height (mm)	H	25
Solid density (kg m^{-3})	ρ	7 800
Young's modulus (MPa)	E	1.561×10^6
Poisson's ratio	ν	0.3
Particles		
Particles number		40 000
Mean particle radius (mm)	R	0.2
Particle radius range (mm)		0.14-0.26
Particle solid density (kg m^{-3})	ρ	680
Poisson's ratio	v	0.35
Yield strength (MPa)	p_y	100
Mean loading (plastic) stiffness (N m^{-1})	k_1	1×10^5
Mean unloading (elastic) stiffness (N m^{-1})	k_2	4×10^5
Mean adhesion stiffness (N m^{-1})	k_c	0; 600
Restitution coefficient	e	0.5
Particle-particle friction coefficient	$\mu_{p\text{-}p}$	0.5
Particle-wall friction coefficient	$\mu_{p\text{-}w}$	0.15
Rolling friction coefficient	m_r	0.01
Bond radius (μm)	r_b	20
Bond tension strength (MPa)	σ_c	3-40
Bond Young's modulus (MPa)	E^b	20-120

Table 3. Bulk density of intact wood, sawdust, and pellets

Material	Intact wood	Sawdust	Pellet
	ρ_{bw} (kg m^{-3})	ρ_{bs} (kg m^{-3})	ρ_{bp} (kg m^{-3})
Beech	640±4a	235.5±6.1a	882.1±18.1a
Birch	550±2a	301.7±6.4b	843.9±4.8b
Oak	675±3b	312.6±5.4b	1 005.8±11.8c
Pine	510±2c	267.9±6.7c	937.8±17.8d
Poplar	420±3d	215.1±4.3d	844.5±11.4b
Willow	400±3e	239.9±5.7a	821.0±19.8b

Mean values in a column followed by the same letter are not significantly different at the 5% level.

The initial height of the sawdust sample in the mould was different for different wood materials which resulted in different initial bulk density values. They were highest for oak and lowest for poplar (Table 3). The bulk density of the sawdust samples ρ_b *vs.* the compressive pressure during the loading-unloading loop is presented in Fig. 3. All loops of the density values during the loading-unloading process were very similar despite the big differences in the initial bulk density for different species of wood material. These differences were very quickly negated by the compaction pressure increase. The maximum mean bulk density of all of the wood sawdust samples at σ_z = 120 MPa was 1 396±23 kg m^{-3}. This density was approximately 5% lower as compared to the solid phase density of the sawdust ρ_s as measured using helium pycnometry (Table 4). This means that during compaction, up to a pressure value of 120 MPa the external pores between the sawdust particles were removed and the majority of the internal pores inside the sawdust particles were closed. The course of the density-compaction pressure relationships that were obtained correspond to the findings of Faberode and O'Callaghan (1986) and Ferrero *et al.* (1991), which indicated that the compaction process can be separated into three characteristic phases with respect to the structural changes of the

Table 4. Density of the solid phase of the intact wood and of the sawdust measured by helium pycnometry

Material	Intact wood (including closed pores)	Sawdust
	ρ_w (kg m^{-3})	ρ_s (kg m^{-3})
Beech	890.1±5a	1 457±1a
Birch	1 370±0.3b	1 465±0.8b
Oak	1 068±1.6c	1 460±1.1a
Pine	1 427±0.3d	1 469±0.6b
Poplar	682.3±1e	1 511±1c
Willow	890.7±5a	1 482±2d

Mean values in a column followed by the same letter are not significantly different at the 5% level.

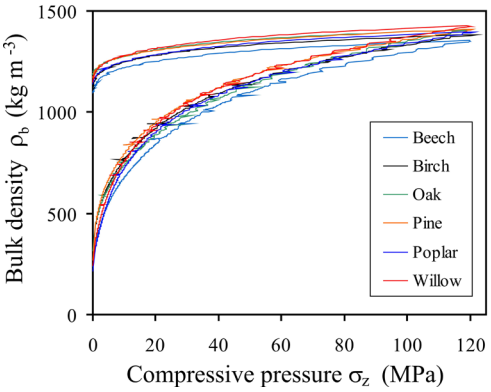

Fig. 3. The loading-unloading loops of the bulk density of sawdust ρb(σz) during the compaction process in a mould.

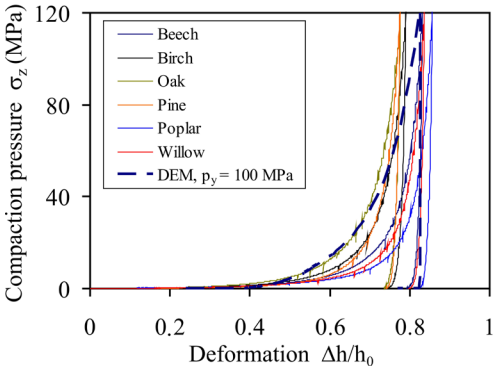

Fig. 4. Stress-deformation dependencies during the compaction-unloading cycle of sawdust in a mould and the DEM simulation fitting.

material: 1) an initial linear phase related to the reduction of free spaces between the sawdust particles, 2) distinctly nonlinear and different for different species (closing intenal pores inside the sawdust particles), 3) elastic behaviour of the sawdust particles (for the bulk density above 1 200 kg m^{-3}).

Unloading resulted in a decrease in the mean bulk density of all wood sawdust samples to approximately 1 144±31 kg m^{-3}. A further decrease in the bulk density of the pellets ρ_{bp} to a final value in the range 800-1 000 kg m^{-3} occurred during the removal of pellets from the mould and relaxation (Table 4). The diameter of the pellet increased to 10.25±0.1 mm after its removal from the mould and remained almost constant during the relaxation time. After seven days of relaxation the height of the pellets increased to 6.05-7.37 mm depending on the wood material used. The lowest height increase occurred for oak and the highest one for willow pellets. No cracks were visible.

The strain, ε_z, applied for the determination of the loading-unloading loop of compaction, $\sigma_z(\varepsilon_z)$, was related to the initial height h_0 of the individual samples of uncompacted sawdust in the mould, $\varepsilon_z = \Delta h/h_0$. With this approach, the stress-strain loops of all wood materials, $\sigma_z(\varepsilon_z)$, were very similar (Fig. 4) despite the difference in the initial height. The loading-unloading curves were approximated by the DEM simulated relationship with the elastic-plastic contact model. The linear elasto-plastic contact model provided an adequate fit of curvature for the experimental loading path comprising three stages of compaction as indicated by Faberode and O'Callaghan (1986). The best fit of the experimental stress-strain curve was provided by the following values of the material parameters: $p_y = 100$ MPa and $e = 0.5$. The shape of the $\sigma_z(\varepsilon_z)$ relationships and the quality of fitting the experimental data corresponded to the quality of the fitting of cyclic loading of pinewood chips obtained from similar DEM simulations performed by Xia *et al.* (2019) for a much lower range of compaction pressures.

Figure 5 illustrates the evolution of the contact force chains during the diametral compression test obtained from DEM simulations. A slice of pellet with a thickness of 1 mm in the centre was selected for the analysis. It may be observed that the chains of the compressive forces initiate in locations close to the loading plates (#1) and as the

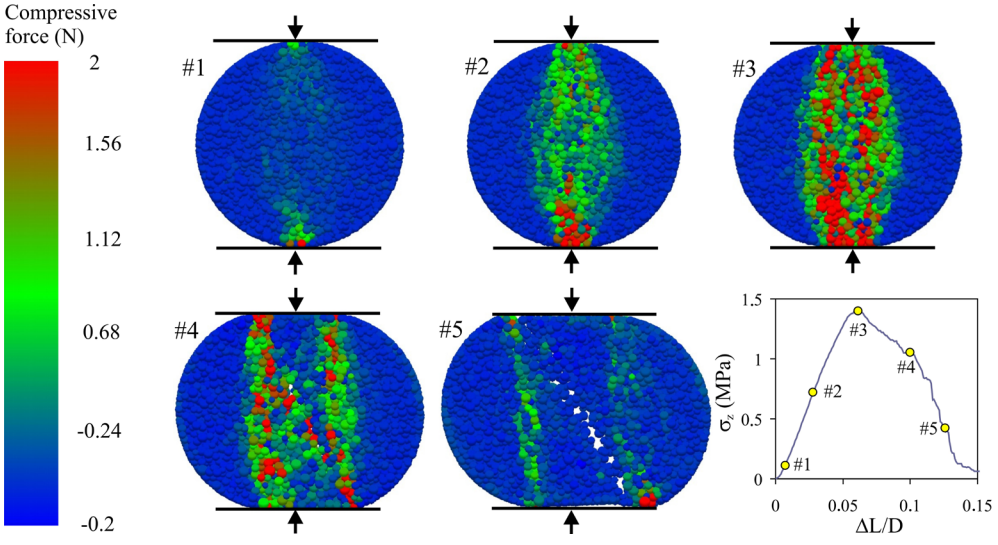

Fig. 5. Visualization of the evolution of the contact force chains during the diametral compression test conducted for the oak pellet.

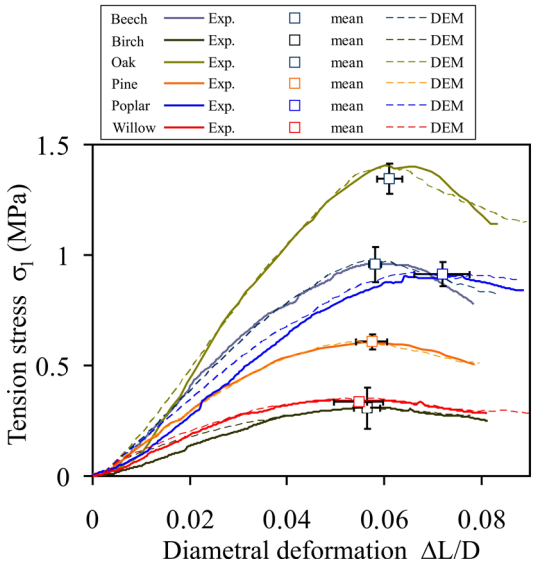

Fig. 6. Fitting the $\sigma_1(\Delta L/D)$ relationships of diametral compression. The bars indicate the SD of the mean values.

deformation progresses, the compressive forces localize into two symmetric, lens-shaped chains along the loading direction (#2). The tension forces were mainly localized outside two chains of the compressive force. The tension forces that occurred between two chains of compressive forces connected them together until the failure point. At the failure point (#3 in Fig. 5) a crack was initiated in the centre of the pellet, *i.e.* in the area of the largest accumulation of broken bonds. After failure (#4 and #5) the compressive force of the two chains weakened and this was followed by the separation of two parts of the broken pellet.

Figure 6 presents the experimental $\sigma_1(\Delta L/D)$ relationships for sawdust pellets produced from the sawdust of six wood materials fitted by the DEM simulated relationships. The tensile strength of the pellets (experimental and modelled) and the best fitting parameters of the DEM simulations are presented in Table 5. All of the $\sigma_1(\Delta L/D)$ relationships revealed the rounded shape of the stress-deformation curve without any sudden pressure drop typical for a ductile breakage mode. The highest tensile strength occurred

Table 5. Tensile strength of pellets (experimental and modelled) and the best fitting parameters of DEM simulations

Material	Exp.	DEM			
	σ_f (MPa)	σ_f (MPa)	E^b (MPa)	σ_c (MPa)	*RRMSE*
Beech	0.958±0.078a	0.974	82	24	0.031
Birch	0.307±0.009b	0.305	36.6	10.1	0.039
Oak	1.346±0.068c	1.402	120	36	0.111
Pine	0.608±0.034d	0.608	50.4	13.5	0.028
Poplar	0.916±0.054a	0.917	68	40	0.145
Willow	0.337±0.015b	0.351	25.9	9	0.032

Mean values in a column followed by the same letter are not significantly different at the 5% level.

for pellets produced from oak and the lowest for pellets produced from birch. The individual experimental stress-deformation relationships that were located the closest to the mean tensile strength point (σ_f, $\Delta L_f/D$) were approximated best by the DEM simulations. The best fitting was obtained for pine pellets (*RRMSE* = 0.028) and the worst for poplar pellets (*RRMSE* = 0.145). The tensile strength values σ_f predicted by the DEM simulations were very close to the experimental values. The values of the bond elastic modulus E^b corresponding to the highest (oak) and the lowest (birch) tensile strength of the pellets were found to be 120 and 36.6 MPa, respectively. The corresponding tensile strength of the bonds σ^c applied to the BPM model of oak and birch pellets was 36 and 10.1 MPa, respectively. The range of values of the bond elastic modulus E^b that were applied to DEM simulations corresponded to the range of values determined experimentally in the puncture test of wood pellets (Gallego *et al.*, 2020). It was found that the relative difference in the values of the bond parameters that were applied to the DEM modelling of pellets made from the sawdust of hard (oak) and soft (birch) wood materials corresponded to the relative difference in the elastic properties of intact wood for those materials presented in the literature (Kretschmann, 2010).

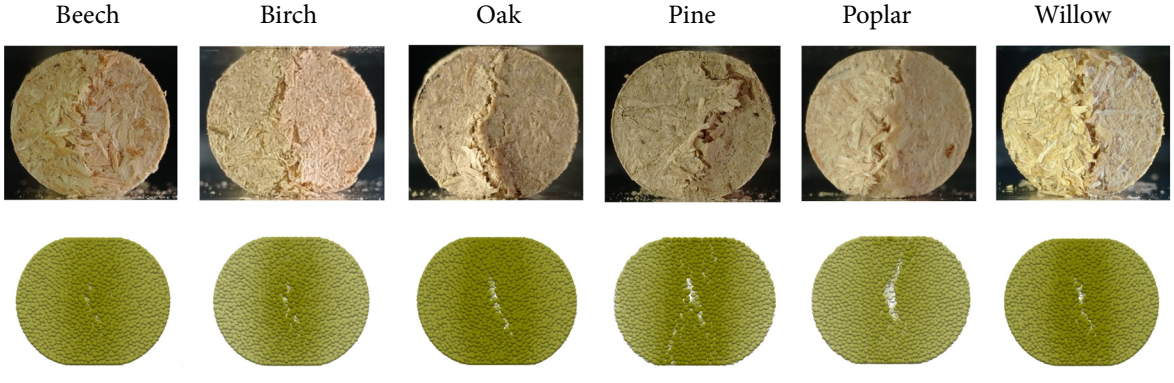

Fig. 7. Experimental and DEM simulated breakage profiles obtained for $\Delta L/D$ = 0.08.

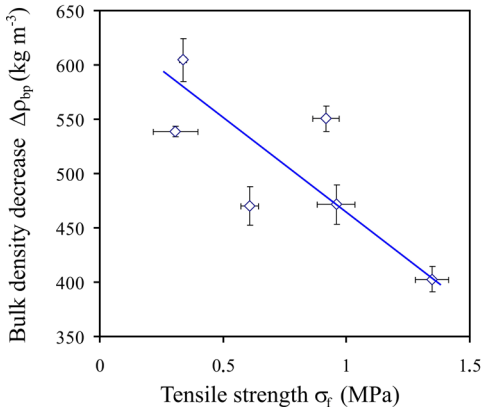

Fig. 8. Decreases in the bulk density of the pellets during unloading and relaxation *vs.* their tensile strength.

The typical experimental breakage profiles of the pellets produced from particular wood materials and the corresponding DEM simulated profiles are presented in Fig. 7. Two types of breakage profiles may be distinguished: 1) a single, straight (oak) or curved (willow), line of breakage or 2) an emerging branch of cracks (pine). The DEM simulated breakage profiles revealed a high degree of similarity to the experimental profiles. In both cases the breakage was initiated in the central part of the pellet and with an increase in deformation propagated towards the loading plates. The inclination of the breakage line to the loading direction did not exceed 25°.

DISCUSSION

The experiments performed in this study indicated that the pellets of sawdust produced that originated from different wood species with the same moisture content, were compacted in strictly controlled conditions up to the same pressure and provided over a four-fold difference in tensile strength between the highest and the lowest strength values. The reason for this is the differing ability of the sawdust particles from different wood species to create particle-particle bonding. A similar tendency was observed in a decrease in the bulk density of the pellets as compared to the maximum bulk density at a compaction pressure of 120 MPa. During unloading, removal from the mould and over the course of the relaxation period, the bulk density of the pellets decreased by approximately 35% (Fig. 2 and Table 3). The greatest decrease in bulk density was obtained in the case of willow pellets (605±20 kg m^{-3}) and the lowest decrease in the case of oak pellets (403±12 kg m^{-3}). Plotting the difference in bulk density between the compacted and relaxed pellet against the tensile strength of the pellet of the particular species of wood in question, it was observed that the higher the tensile strength the lower the decrease in bulk density (Fig. 8). This finding coincides with the findings of Larsson and Samuelsson (2017) thereby indicating that the tensile strength of the pellets increased with their density and durability. This relationship results directly from the physical interactions between the sawdust particles responsible for the creation of the binding forces. The binding forces are generated during the compaction process. During unloading, removal from the mould and over the course of the relaxation period, some of the bonds broke due to elastic recovery. Elastic recovery increases the distance between the sawdust particles and destroys some of the bonds. The greater the bonding force created during compaction the lower the density decrease during unloading. Only the final strength of a relaxed pellet may be determined experimentally, while the maximum strength of a compacted pellet can only be approximated from other measurements.

DEM modelling provides some possibilities for achieving a deeper insight into the process of bond creation during compaction and its breakage during unloading. For an assumed value of the solid density of particles that is equal to the intact wood bulk density of 680 kg m^{-3} the DEM simulations indicated that during unloading, removal from the mould and relaxation, the coordination number of the pellet sample decreased from its maximum value of 14.1 at σ_z =120 MPa to 12.9 after pellet relaxation, and the bulk density decreased from 1 350 kg m^{-3} to 1 100 kg m^{-3}. The reduction in the coordination number (~9%) was much lower as compared to the reduction in the bulk density (~18%) due to the very high level of the ratio of the mean normal overlap δ_n to the particle radius r (~0.42) at a compaction pressure of 120 MPa which decreased to δ_n/r~0.33 in the relaxed pellet. Such a high level of overlap was necessary in order to reproduce a high level of the deformation of the sawdust particles and also to flatten the contact areas during compaction.

A bond radius of 20 μm corresponded to the findings of an SEM analysis as presented by Horabik *et al*. (2021). This value of bond radius consisted of a small fraction (~15%) of the particle-particle contact radius. The applied value of the bond radius allowed for an accurate prediction of the stress-deformation relationships for pellets produced using all wood species with a reasonable range of values of the elastic parameters of their bonds. The order of magnitude of the elastic parameters of bonds are similar to the values applied by Xia *et al*. (2019) and Gilvari *et al*. (2020) for the DEM modelling of the breakage strength of wood pellets.

The main novelty of this study was the attainment of a fairly good quality numerical reproduction of the experimental relationships between the compaction process and the diametral compression test using the elastic-plastic contact model. The shape of the $\sigma_1(\Delta L/D)$ relationship during the diametral compression test, the tensile strength, the strain at the point of failure, and also the breakage profiles were well reproduced in the DEM simulations. The tendency for a decrease to occur in the difference between the density of a compacted and relaxed pellet with a corresponding increase in the strength of the pellet was interpreted from the point of view of particle-particle interactions.

CONCLUSIONS

1. The highest value of breakage strength was obtained for oak pellets and the lowest one for birch pellets. The highest value breakage strength was over four times higher than that of the lowest one.

2. The difference between the bulk density of the compacted and the relaxed pellet decreased with increases in the breakage strength of the pellet.

3. DEM simulations that were equipped with the elastic-plastic contact model and the bonded particle model accurately reproduced the diametral compression test of the pellets examined and provided a qualitative and quantitative agreement with the experimental data.

Conflict of interest: The Authors declare they have no conflict of interest.

REFERENCES

Cundall P.A. and Strack O.D., 1979. A discrete element model for granular assemblies. Géotechnique, 29, 47-65, https://doi.org/10.1680/geot.1979.29.1.47

DEM Solutions Ltd. EDEM 2018.2. Documentation, Copyright© 2018.

Faberode M.O. and O'Callaghan J.R., 1986. Theoretical analysis of the compression of fibrous agricultural materials. J. Agric. Eng. Res., 35(3), 175-191, https://doi.org/10.1016/S0021-8634(86)80055-5

Ferrero A., Horabik J., and Molenda M., 1991. Density − pressure relationship in compaction of straw. Can. Agric. Engin., 33, 107-111.

Gallego E., Fuentes J.M., Ruiz Á, Hernández-Rodrigo G., Aguado P., and Ayuga F., 2020. Determination of mechanical properties for wood pellets used in DEM simulations. Int. Agrophys., 34, 485-494, https://doi.org/10.31545/intagr/130634

Gilvari H., de Jong W., and Schott D.L., 2020. Breakage behavior of biomass pellets: an experimental and numerical study. Comput. Part. Mech., 8, 1047-1060, https://doi.org/10.1007/s40571-020-00352-3

Hehar G., Fasina O., Adhikari S., and Fulton J., 2014. Ignition and volatilization behavior of dust from loblolly pine wood. Fuel Process., 127, 117-123, https://doi.org/10.1016/j.fuproc.2014.04.036

Horabik J., Bańda M., Józefaciuk G., Adamczuk A., Polakowski C., Stasiak M., Parafiniuk P., Wiącek J., Kobyłka R., and Molenda M., 2021. Breakage strength of wood sawdust pellets: Measurements and modelling. Materials, 14, 3273, 1-25, https://doi.org/10.3390/ma14123273

Huang Y.J., Nydal O.J., and Yao B., 2014. Time step criterions for nonlinear dense packed granular materials in time-driven method simulations. Powder Technol., 253, 80-88, https://doi.org/10.1016/j.powtec.2013.10.010

Ilic D., Williams K., and Ellis D., 2018. Assessment of biomass bulk elastic response to consolidation. Chem. Eng. Res. Des., 135, 185-196, https://doi.org/10.1016/j.cherd.2018.05.028

Kaliyan N. and Morey R.V., 2009. Factors affecting strength and durability of densified biomass products. Biomass Bioenerg., 33, 337-359, https://doi.org/10.1016/j.biombioe.2008.08.005

Kaliyan N. and Morey R.V., 2010. Natural binders and solid bridge type binding mechanisms in briquettes and pellets made from corn stover and switchgrass. Bioresour. Technol., 101, 1082-1090, https://doi.org/10.1016/j.biortech.2009.08.064

Kretschmann D.E., 2010. Mechanical properties of wood. In Wood handbook. Wood as engineering material. General Technical Report FPL-GTR-190, 2nd ed.; WI: U.S. Department of Agriculture, Forest Service, Forest Products Laboratory, Madison, 5.1-5.46.

Larsson S.H. and Samuelsson R., 2017. Prediction of ISO 17831-1:2015 mechanical biofuel pellet durability from single pellet characterization. Fuel Process. Technol., 163, 8-15, https://doi.org/10.1016/j.fuproc.2017.04.004

Luding S., 2005. Shear flow modelling of cohesive and frictional fine powder. Powder Technol., 158, 45-50, https://doi.org/10.1016/j.powtec.2005.04.018

Mahajan A., Dafnomilis I., Hancock, V., Lodewijks G., and Schott D., 2017. Assessing the representativeness of durability tests for wood pellets by DEM Simulation - Comparing conditions in a durability test with transfer chutes. EPJ Web Conf., 140, 15004, https://doi.org/10.1051/epjconf/201714015004

Molenda M., Horabik J., Parafiniuk P., Oniszczuk A., Bańda M., Wajs J., Gondek E., Chutkowski M., Lisowski A., Wiącek J., and Stasiak M., 2021. Mechanical and combustion properties of agglomerates of wood of popular Eastern European species. Materials, 14, 2728, 1-14, https://doi.org/10.3390/ma14112728

Potyondy D.O. and Cundall P.A., 2004. A bonded-particle model for rock. Int. J. Rock Mech. Min. Sci., 41, 1329-1364, https://doi.org/10.1016/j.ijrmms.2004.09.011

Rackl M., Top F., Molhoek C.P., and Schott D.L., 2017. Feeding system for wood chips: A DEM study to improve equipment performance. Biomass Bioenerg., 98, 43-52, https://doi.org/10.1016/j.biombioe.2017.01.003

Shaw M.D., Karunakaran C., and Tabil L.G., 2009. Physicochemical characteristics of densified untreated and steam exploded poplar wood and wheat straw grinds. Biosyst. Eng., 103, 198-207, https://doi.org/10.1016/j.biosystemseng.2009.02.012

Song X., Zhang S., Wu Y., and Cao Z., 2020. Investigation on the properties of the bio-briquette fuel prepared from hydrothermal pretreated cotton stalk and wood sawdust. Renew. Energy, 151, 184-191, https://doi.org/10.1016/j.renene.2019.11.003

Stasiak M., Molenda M., Bańda M., Wiącek J., Parafiniuk P., and Gondek E., 2017. Mechanical and combustion properties of sawdust - Straw pellets blended in different proportions. Fuel Process. Technol., 156, 366-375, https://doi.org/10.1016/j.fuproc.2016.09.021

Tsuji Y., Tanaka T., and Ishida T., 1992. Lagrangian numerical simulation of plug flow of cohesionless particles in a horizontal pipe. Powder Technol., 71, 239-250, https://doi.org/10.1016/0032-5910(92)88030-L

Walton O.R. and Braun R.L., 1986. Viscosity, granular temperature, and stress calculations for shearing assemblies of inelastic, frictional disks. J. Rheol., 30, 949-980, https://doi.org/10.1122/1.549893

Whittaker C. and Shield I., 2017. Factors affecting wood, energy grass and straw pellet durability - A review. Renew. Sust. Energ. Rev., 71, 1-11, https://doi.org/10.1016/j.rser.2016.12.119

Xia Y., Lai Z., Westover T., Klinger J., Huang H., and Chen Q., 2019. Discrete element modeling of deformable pinewood chips in cyclic loading test. Powder Technol., 345, 1-14, https://doi.org/10.1016/j.powtec.2018.12.072